Lunar Tides in Loch Ness, Scotland

David T. Pugh[1], Philip L. Woodworth[1] , and Machiel S. Bos[2]

[1] National Oceanography Centre, Joseph Proudman Building, 6 Brownlow Street, Liverpool L3 5DA, UK.

[2] CIMAR/CIIMAR, University of Porto, Rua dos Bragas, 289, 4050-123 Porto, PORTUGAL

* Emails: d.pugh@mac.com, plw@noc.ac.uk and mbos@ciimar.up.pt. Correspondence for the submission should be addressed to PLW. Main science contact is DTP.

Abstract

Measurements have been made of the astronomical tide in Loch Ness, Scotland, which is not directly connected to marine tides. Our measurements of the loch tide are, so far as we know, the first in a European lake where the tide originates primarily from ocean tide loading. Loch Ness is a readily accessible lake and is in a region for which the neighbouring ocean tides are large and described well by modern global ocean tide models The principal tidal constituent, M_2, was observed to have an amplitude of approximately 1.5 mm, and to be in anti-phase, at each end of the loch. These values are in close agreement with the theoretical combined effects of the direct gravitational tide (body tide) and the tilt effects due to ocean tide loading, computed using Green's functions based on conventional elastic-Earth models. By analyzing over long-periods for coherent tidal signals, we are able to significantly improve the signal-to-noise ratio in the tilt values compared with values obtained by direct level differencing. Our tilt accuracy of better than 10^{-8} , measured over 35km, demonstrates Loch Ness as one the world's longest and most accurate tiltmeters. Despite this unprecedented accuracy, Earth tidal models are still at least as accurate as our ability to measure them.

1 1. Introduction

2

3 Loch Ness, located along the Great Glen fault, in the north of Scotland, is
4 approximately 37 km long, has an average width of 1.6 km, and a maximum depth of
5 227 m. It aligns 38° east of north, approximately southwest to northeast, and at its
6 northern end is connected to the tidal Moray Firth and North Sea, by a short (~13 km)
7 length of the River Ness. At 16 m above mean sea level, Loch Ness is not directly
8 influenced by the ocean tide. However, we have been able to observe small (mm)
9 tides in the Loch due to direct gravitational tidal attraction, and due to the loading of
10 the solid earth by the ocean tides of the adjacent seas. This is believed to be the first
11 observation in a European lake of an astronomical tide primarily due to loading.

12

13 Recent studies [*Richter et al.*, 2009] have suggested that for Lake Fangano in Tierra
14 del Fuego, the observed small tides are not consistent with the theoretical combined
15 direct and loading tidal effects. This conclusion has been challenged [*Bos*, 2010;
16 *Richter et al.*, 2010] by the suggestion that the tidal loading computations have large
17 uncertainties. Loch Ness is an accessible long freshwater lake for which the tidal
18 loading calculations can be performed with great accuracy because the tides around
19 northwest Europe are observed and modelled well. We show from our analyses that
20 the tides in Loch Ness are consistent with the known direct and loading effects, to a
21 much higher degree of accuracy than was possible for Tierra del Fuego.

22

23 Geologically the Great Glen fault is a strike-slip fault that divides the Scottish
24 Highlands, and can be traced through the Moray Firth into the North Sea. There are
25 still occasional moderate earthquakes in the region, notably in November 1890 and

September 1901. Deep-seated crustal inhomogeneities are reflected in local gravity and magnetic anomalies and in seismics [*Trewin*, 2008; *Mendum and Noble*, 2010; *Nicolson et al.*, 2011]. Geothermal heat flow is normal in the sediments of Loch Ness, with higher values in the region of the Foyers granites [*Pugh*, 1977]. The Loch itself has been formed and deepened by glacial excavation.

Several studies of the water levels and temperatures in Loch Ness were made in the late nineteenth-century [*Murray and Pullar*, 1910], establishing that there is a natural period of seiching for Loch Ness of around 32 minutes. More recently, internal waves of period somewhat greater than 2 days have been observed during the summer stratification [*Thorpe*, 1971]; the Loch is well mixed vertically in winter. During the period of our intensive observations, April-October 2010, the Loch level had a range of 0.7 m, dominated by precipitation and river flow; more extreme levels occur during flood and drought. We have not attempted a full analysis of causes for Loch water level changes: seiching, rainfall, wind set-up, upwelling and steric adjustments, such as that done for example, for Lake Kariba [*Ward*, 1977] . In passing we note from our measurements that after a storm on 21 August 2010, the surface water temperatures at Fort Augustus at the southern end of Loch Ness fell rapidly from 14.0 to 6.9 ^{0}C, presumably due to upwelling and the sub-thermocline waters breaking the surface; recovery took place slowly over the next 36 hours. Here we concentrate on the relatively miniscule (mm), regular tidal changes in Loch levels.

2. Lake Tide Measurements

Tides have been measured in many lakes unconnected to the sea [*Hutchinson*,

1957; *Defant*, 1961; *Melchior*, 1983]. These have included Lakes Baikal [*Grace*, 1931], Michigan and Superior [*Mortimer and Fee*, 1976], Kariba [*Ward*, 1977] and Tanganika [*Melchior*, 1956]. Lake Constance provides the only example known to us of astronomical tides measured in a European lake [*Hamblin et al.*, 1977]. Melchior [1983] explains that the tidal forcing can be both directly gravitational, and indirectly due to marine tidal loading, resulting in crustal tilting. The tides in all of these lakes are substantially due to the direct gravitational attraction of the Moon and Sun and not to loading.

The recent tidal measurements in Lake Fangano, by contrast, are additionally strongly influenced by tidal loading, leading the authors [*Richter et al.*, 2009] to propose that tidal measurements in lakes can in suitable circumstances be used to help define the Green's function that represents the local crustal elastic response. An alternative interpretation [*Bos*, 2010] of the observed differences from standard crustal model predictions [*Baker*, 1980], suggests that the discrepancies are due to inadequate load modelling. Our motivation for the Loch Ness tidal measurements was to see whether, in circumstances of well-modelled and large local tidal loading, the standard Green's function models for tilt are indeed correct. Although we compute the tidal loading using the gravitational potential Green's function, by taking the difference we are testing the Green's function for tilt. We have adopted the additional powerful approach of analyzing for tides in the differences in widely spaced observations, recognizing that differencing removes most of the large background variations in Loch levels and atmospheric pressure variations: if the levels are analysed as *differences* then the lakes become effectively very sensitive crustal tilt meters (for crustal studies see, for example, [*Mueller et al.*, 1989]). Tilts are more

sensitive than vertical displacements to local crustal loading and can be accurately measured over long baselines [*Baker*, 1980]. In the event, we were able to measure gradients to better than one part in 10^8 i.e. to approximately one tenth of a millimetre over a 35 km length of the Loch.

3. The Loch Ness Tidal Measurements

We made sub-surface pressure measurements, using pressure sensors that record water level pressure plus atmospheric pressure, at five sites along Loch Ness (Table 1(a), Figure 1). We used Richard Branker Research pressure gauges (RBR 450) fitted with aneroid pressure sensors set to record every 10 minutes. Their pressure measurements were calibrated at the National Oceanography Centre (NOC) Holyhead coastal tide gauge station, where sea water density could be estimated adequately, and adjusted subsequently for freshwater density for use in Loch Ness. All measurements reported here were made over a common 201 day period between noon day 98 (8 April) 2010 and noon day 299 (26 October) 2010. An RBR gauge at Foyers (denoted FO in Figure 1) was lost, but we had access to data from an adjacent Vega acoustic water level gauge operated by the hydro-electric station. We also had data from a Scottish Environment Protection Agency (SEPA) float and stilling well gauge, located below the flight of locks at Fort Augustus (denoted FAS), and a short distance from our own Fort Augustus (FA) RBR pressure sensor. The FA record was corrected for seven small jumps, each between 0.04 and 0.20 m, probably due to gauge movement on the lake bed, evident by comparison to the other three RBR gauges. Measurements from all sensors were filtered to provide hourly values, and a

101 Doodson X0 filter (Pugh, 1987) used to remove the high variance in the time series
102 due to low frequency changes in the loch. Tidal parameters were then computed using
103 the Tidal Analysis Software Kit (TASK-2000) package of NOC [*Bell et al.*, 1996].
104 Standard errors on the amplitudes and phase lags of each constituent were determined
105 from the scatter of analyses of independent monthly blocks of data (Table 1b).
106
107 The existence of genuine astronomical tidal signals in the records can be
108 demonstrated effectively using our pressure records from the NE and SW ends of the
109 Loch at Aldourie (denoted AL in Figure 1) and Fort Augustus (FA) respectively.
110 Figures 2 (a,b) shows power spectra for the average and difference of the two time
111 series respectively. Figure 2(a) represents daily variations in average Loch level,
112 primarily due to hydro-electric pumping of water between Loch Ness and
113 neighbouring lochs. This results in a spectrum dominated by the S_1 constituent and its
114 harmonics, while any variability at the M_2 frequency, which has opposite phase at the
115 two ends of the Loch, cancels out. On the other hand, Figure 2(b) shows clear M_2, S_2
116 and N_2 signals in the pressure-difference record. These will all be of astronomical
117 tidal origin, with the coherent variations at S_1 and S_2, originating from the hydro-
118 electric pumping and other uses of the loch, cancelling out. Although the
119 unambiguous tidal components stand out above the continuum of Loch variability,
120 attempts have been made to reduce the background further with the use of regressions
121 involving along- and cross-loch air pressure gradients with only moderate success.
122
123 The ability to demonstrate clear tidal signals in the pressure-difference record
124 is thanks to the stability of the RBR instruments to within a few cm over several
125 months during which Loch level varied by 0.70 m. For the best pair (**DR-TB**) which

126 are 17.5 km apart, the standard deviation of 10-minute pressure difference, which
127 includes contributions from Loch dynamics as well as instrumental errors, was only
128 4.6mm. Higher values were obtained for other pairs due to the jumps at FA referred to
129 above and a long-term drift at AL.
130
131 Table 1(b) shows the M_2, S_2 and N_2 semidiurnal tidal constituents at the six
132 places along the Loch. The S_2 constituent is the largest and is simultaneous to within
133 an hour over the whole Loch, demonstrating that the Loch adjusts rapidly and
134 synchronously to water volume changes, given its short natural period of oscillation
135 (32 minutes). This S_2 term is primarily a harmonic of the daily cycle of pump storage
136 cycling at the Foyers hydro-electric station, and as such makes direct solar tide
137 analysis impossible (Figure 2a). The S_1 constituent amplitude and Greenwich phase
138 lag at Foyers were found to be 19.6 mm and 166^{0}; these values, from a year of data to
139 day 299 2010, are equivalent to a cycle of water exchange of $1.1*10^{6}$ m^3, with
140 maximum Loch levels around 2300 GMT. The N_2 amplitudes are very small and its
141 phases are ill-defined, but the M_2 amplitudes and phases show a clear pattern of
142 variation along the Loch with maximum values at the two ends, and 157^{0} out of
143 phase. Note that the pressure gauges include the small S_2 tide in atmospheric pressure
144 (for the 6-month period, air pressure S_2 amplitude and phase lag were 0.24 +/- 0.015
145 mbar and 311.6 +/- 3.5 ° respectively). Figure 3a shows a clear trend in the M_2 vector
146 plot along the Loch; the four pressure gauges include a very small signal of M_2 in
147 atmospheric pressure (0.01 +/- 0.01 mbar) which may account for part of the slight
148 offset of the fitted line from the origin. The FAS amplitude is smaller than expected,
149 which may be due to either the position of the gauge in a confined area of water
150 beneath the canal locks at the SW end of the Loch, or to the unsuitability of the gauge

151 type (float gauge) for measuring the small tidal signals.

152

153 As demonstrated above, there are significant advantages in using a pair of
154 pressure gauges at each end of the Loch as an effective tilt meter. The tilt is defined as
155 $\Delta h/L$, where Δh is the observed tidal change in water levels at the opposite ends of the
156 Loch, and L is the distance between the sites (Table 2). As the M_2 phases are almost
157 opposite at each end, the tidal signal measured in the difference signal has twice the
158 amplitude of that in the individual records. In addition, any background noise from air
159 pressure variations and non-tidal Loch level changes is eliminated, resulting in
160 measured gradients representative of those due to loading (Figure 2b). Also, gradients
161 are more sensitive to local crustal loading effects [*Agnew*, 2007].

162

163 Table 2 shows the results of analyzing for M_2 , S_2 and N_2 in the differences in
164 levels for pairs **AL-FA** (the extreme ends) and **TB-FA, DR-TB,** and **AL-DR**, within
165 the Loch. The results are remarkably consistent, in both amplitude and phase, with an
166 along–Loch amplitude gradient of 0.090 +/- 0.004 mm per km for M_2. Once the
167 Loch-coherent part of S_2 has been removed by the differencing, a gradient value
168 which is 0.31 of that of M_2 remains, close to the S_2 /M_2 ratio of amplitudes in the
169 adjacent seas, and with an implied age of the tide of 46 hours [*Pugh*, 1987]. For
170 comparison, at Invergordon in the Moray Firth, the ratio is 0.35, and the tidal age is
171 38 hours derived from tidal constants in the NOC Applications Group data bank. Even
172 N_2 is now much more stable, with an amplitude ratio to M_2 of 0.26 compared to 0.20
173 at Invergordon. (For comparison, in the Equilibrium Tide the S_2 /M_2 and N_2 /M_2
174 amplitude ratios are 0.46 and 0.19 respectively). The overall Loch gradient for M_2,
175 represented by the difference **AL-FA,** has an amplitude of 3.12 +/- 0.13 mm and a

phase lag of 307.5 +/- 2.3^0 .

4. Interpretation of Measurements

The direct M_2 tides in the earth in metres due to gravitational forcing (the tide generating potential) can be written [*Pugh*, 1987]:

$$0.69 \times 0.244 \times \cos^2 D_l \times \cos 2C_p$$

where the 0.69 is a solid Earth elastic response factor (diminishing factor), the 0.244 is the Equilibrium Tide amplitude (in metres) of M_2, D_l is the latitude, and C_p is the hour angle which cycles once per lunar day. The gradients in the direct gravitational tides along the Loch, obtained by differencing the above formula at the AL and FA sites have two components: the first is in quadrature with the lunar transit due to east-west effects; the second, due to the latitude term $\cos^2 D_l$ is in phase with lunar transit. The combined effect of these is an M_2 tide of amplitude 0.9 mm and phase lag 229^0.

Tidal loading is due to the potential field created by the Earth's elastic deformation under the weight of the ocean tide plus the self potential of the tidal waters being considered. Table 3 summarises the tidal gravitational potential loading for M_2 calculated using four different ocean tide models by methods described elsewhere [*Farrell,* 1973; *Bos and Baker*, 2005; *Penna et al.*, 2008] and Green's functions derived from the Preliminary Earth Reference Model (PREM) [*Dziewonski et al.*, 1981; *Bos*, 2010]. The four chosen models were FES2004, TPXO7.2, GOT4.7 and EOT08a, all of them quite recent and therefore presumably more accurate than

older ones [*Lyard et al.*, 2006; *Egbert and Erofeeva*, 2002; *Ray*, 1999; *Savcenko and Bosch*, 2008. Note that TPXO7.2 and GOT4.7 are recent developments of the models described in the references]. Loading due to tides in the Loch itself, computed using the numerical model described below, was found to be negligible.

The method of *Bos and Baker* [2005] for the recursive definition of model grid cells around the complicated Scottish coastline is demonstrated by Figure 4. The NE end of Loch Ness at Aldourie, indicated by the blue cross, is only ~13 km from the open sea (the Beauly and Moray Firths). A tidal loading calculation at its location clearly requires densification of the grid normally employed for ocean tide modelling. In this case, the refinements started with the original ocean tide model grids (0.125° x 0.125° for FES2004, TPXO.7.2 and EOT08a and 0.25° x 0.25° for GOT4.7). The grid cells for each model near to the coastline were divided recursively into 4 smaller ones, until a good fit was obtained with the coastline (defined by the shoreline data base of *Wessel and Smith*, 1996). Another criterion was that the size of the grid cell cannot be too large to violate the assumption that the weight of the tides inside the cell looks like a point load [*Farrell*, 1972]. For this reason, some other cells in the open sea near Loch Ness were subdivided. The resulting finest grid resolution was approximately 0.01° x 0.01° (approximately 0.6 x 1.1 km).

Using a potential Green's function with extreme modified upper 5 km characteristics [*Bos*, 2010], gives very small changes of the order of 0.01 mm and 0.1 degrees at the gauges, confirming that the effect of variations in the elastic properties of the upper crust is negligible (cf. [*Baker,* 1980]).. Table 3 shows that M_2 difference between the two ends of the Loch due to loading has a value of 2.94 mm in amplitude

226 and 323.0 ^{0} in Greenwich phase lag, based on an average of the four models. We
227 estimate an uncertainty of 3% in amplitude in these model results due to grid
228 resolution, seasonal and nodal M_2 adjustments and sea-water density uncertainties.
229
230 The main aim of our experiment was to see whether the observed tidal tilt for
231 M_2 for Aldourie minus Fort Augustus (AL-FA) of 3.12 +/- 0.13 mm amplitude and
232 307.5+/- 2.3^{0} phase lag (Table 2) was consistent with the above combined direct and
233 tidal loading components. The results are summarized in Figure 3b. The agreement is
234 good to ~5% or within one standard error in the observed M_2 difference-signal
235 (gradient).The phase lag agreement is best for the GOT4.7 model. We believe that
236 disagreements are within the measurement and modelling errors, as shown by the
237 overlap of the circles in the figure. We note also that, despite this being an area of
238 strong crustal inhomogeneities [*Trewin*, 2008], the standard Green's functions provide
239 good results
240
241 5. Numerical Model of the Loch
242
243 As M_2 has a period considerably larger than those of the free modes of the loch, the
244 M_2 spatial distribution should be similar to that of the combined potential described
245 above, and tidal dynamics should play only a small role. To test this possibility, a
246 two-dimensional numerical model of the loch was constructed based on tide-surge
247 code used at NOC [*Flather et al.*, 1998]. The model has a spatial resolution of
248 0.000282 x 0.0005° (17 x 56 m), in order to adequately resolve the width of the loch,
249 and a time step of 0.2 seconds. In some model runs, depths were set equal to the loch
250 average of 132 m, in others a close approximation of the real loch bathymetry was

used [*Murray and Pullar*, 1910]; this choice had no effect on model outputs. Bottom friction and horizontal eddy viscosity parameters were selected within a range of generally accepted values; such choices also did not affect outputs. Figure 5 presents typical model findings indicating a largely standing wave character, with M_2 difference between the two ends consistent with expectations from the applied potential, and with a clockwise amphidromic system in the middle. This exercise confirmed that a comparison of measurements to direct gravitational and loading potentials as in Figure 3b is a valid one. Amplitudes and phases from this model were used to confirm that the self-loading due to Loch Ness tides mentioned above is negligible.

6. Conclusions

Our measurements, the first to our knowledge in a European lake where loading is primarily responsible for the tide, demonstrate that consistency with ocean tide information is possible where the ocean tides are themselves well modelled. We have shown that measurements of tidal tilts in lakes can be accurate to better than one part in 10^8, given stable instrument conditions, and that this tilt accuracy is better than the best accuracy for measuring gradients using modern geodetic techniques, for example GPS [*Allinson et al.*, 2004]. Consequently, tidal measurements in other coastal lakes may be useful in validating ocean tide models in locations where ocean models are less precise.

Acknowledgements

We thank the landowners of each site for permission to install our equipment. The Scottish Environment Protection Agency (SEPA) and Scottish and Southern Energy (SSE) kindly made water level data available to us. Mr. Peter Foden and Prof. Trevor Baker (National Oceanography Centre) provided expert technical and scientific advice on our measurements and analysis. We thank Drs. Duncan Agnew and Andreas Richter and a third reviewer for their valuable suggestions. This work was funded by the UK Natural Environment Research Council (NERC).

References

Agnew, D. (2007), Earth tides. pp 163–195 in: Herring, T. (ed) *Treatise on Geophysics: Geodesy*, Elsevier, Amsterdam and Boston, Mass., USA..

Allinson C.R., P.J. Clarke, S.J. Edwards, M.A. King, T.F. Baker, and P.R. Cruddace (2004), Stability of direct GPS estimates of ocean tidal loading, *Geophys. Res. Lett.,* **31**, L15603, doi:10.1029/2004GL020588.

Baker, T.F. (1980) Tidal tilt at Llanrwst, North Wales: tidal loading and Earth structure, *Geophys. J. Roy. Astr. Soc*., 62, 269-290.

Bell, C., J.M. Vassie, and P.L. Woodworth (1996), The Tidal Analysis Software Kit (TASK). (1996) (www.psmsl.org/train_and_info/software).

Bos, M.S., and T.F. Baker (2005), An estimate of the errors in gravity ocean tide loading computations, *J. Geod*esy, 79, 50–63.

Bos,, M.S. (2010), Comment on "Anomalous ocean load tide signal observed in lake-level variations in Tierra del Fuego" by A. Richter et. al., *Geophys. Res. Lett*., **37,** L04303, doi:10.1029/2009GL041531.

Defant, A. (1961), *Physical Oceanography, Volume 2,* Pergamon Press, Oxford, U.K.

Dziewonski, A. M., and D. L. Anderson (1981), Preliminary reference Earth model, *Phys. Earth Planet. Inter*., 25, 297–356.

Egbert, G.D., and S.Y. Erofeeva (2002), Efficient inverse modeling of barotropic ocean tides, *J. Atmos. Oceanic Technol.,* 19, 183-204.

Farrell, W.E. (1972), Deformation of the Earth by surface loads, *Rev. Geophys. Space Phys*., 10(3), 761-797.

Farrell, W.E. (1973), Earth tides, ocean tides and tidal loading, *Phil. Trans. R. Soc. Lond. A*, 274, 253-259.

Flather, R.A., J.A. Smith, J.D. Richards, C. Bell, and D.L. Blackman (1998), Direct estimates of extreme storm surge elevations from a 40 year numerical model simulation and from observations, *Global Atm. Oc. System,* 6, 165-176.

Grace, S.F. (1931), The semi-diurnal lunar tidal motion of Lake Baikal and the derivation of the earth-tides from the water-tides, *Geophys. J. Roy. Astr. Soc.,* 2, 301-309.

Hamblin, P.F., R. Mühleisen, and U. Bösenberg, (1977), The astronomical tides of Lake Constance, *Deut. Hydrograph. Z*., Jahrgang 30, Heft 4, 105-116.

Hutchinson G.F. (1957), *A treatise on limnology*, John Wiley, New York, USA.

Lyard, F., F. Lefevre, T. Letellier, and O. Francis (2006), Modelling the global ocean tides: modern insights from FES2004, *Ocean Dyn.,* 56, 394–415.

Melchior, P.J. (1956), Sur l'effect des marées terrestres dans les oscillations du niveau du Lac Tanganika à Albertville.,*Bulletin de la Classe des Sciences, Académie Royale de Belgique*, 42, 368-371.

Melchior, P. (1983), *The Tides of Planet Earth,* Pergamon Press, Oxford, U.K.

Mendum, J.R., S.R. Noble (2010), Mid-Devonian sinistral transpressional movements on the Great Glen Fault: the rise of the Rosemarkie Inlier and the Acadian Event in Scotland, *Geological Society, London, Special Publications*, 335, 161-187.

Mortimer, C.H., and Fee, E.J. (1976), Free surface oscillations and tides of Lakes Michigan and Superior, *Phil. Trans. R. Soc. Lond. A.*, 1281, 1-61.

Mueller, R.J., M.J.S. Johnston, G.D. Myren, and T. Murray (1989), Lake level observations to detect crustal tilt: San Andreas Lake, California, 1979-1989, *Geophys. Res. Lett.*, 16, 661-664.

Murray, J. and Pullar, L. (1910), *Bathymetrical survey of the Scottish fresh-water lochs.* Volume 1, Challenger Office, Edinburgh, U.K. 785pp.

Nicolson, H., A. Curtis, B. Baptie, and E. Galetti (2011), Seismic interferometry and ambient noise tomography in the British Isles, *Proc. Geol. Assoc.*, (in press), doi:10.1016/j.pgeola.2011.04.002.

Penna, N.T., M.S. Bos, T.F. Baker, and H-G. Scherneck (2008), Assessing the accuracy of predicted ocean tidal loading displacement values.,*J. Geodesy,* 82, 893-907.

Pugh, D.T. (1977), Geothermal gradients in British lake sediments, *Limnol. Oceanogr.,* 22, 581-596.

Pugh, D.T. (1987), *Tides, surges and mean sea level*, John Wiley, Chichester, U.K..

Ray, R.D. (1999), A global ocean tide model from Topex/Poseidon altimetry: GOT99. NASA Technical Memorandum 209478, Goddard Space Flight Center, Maryland, 58 pp.

Richter, A., J. L. Hormaechea, R. Dietrich, R. Perdomo, M. Fritsche, D. Del Cogliano, G. Liebsch, and L. Mendoza (2009) Anomalous ocean load tide signal observed in lake-level variations in Tierra del Fuego, *Geophys. Res. Lett*., 36, L05305, doi:10.1029/2008GL036970.

Richter, A., J. L. Hormaechea, R. Dietrich, R. Perdomo, M. Fritsche, D. Del Cogliano, G. Liebsch, and L. Mendoza (2010), Reply to comments by M.S.Bos on **"**Anomalous ocean load tide signal observed in lake-level variations in Tierra del Fuego", *Geophys. Res. Lett*., 37, L04304, doi:10.1029/2009GL041981.

Savcenko, R., and W. Bosch (2008), EOT08a - Empirical ocean tide model from multi-mission satellite altimetry. Deutsches Geodätisches Forschungsinstitut (DGFI),

Munich, Report Number 81.

Thorpe, S.A. (1971), Asymmetry of the internal seiche in Loch Ness, *Nature,* 231, 306-308.

Trewin, N.H. (Ed) (2008), *Geology of Scotland 4th Edition,* Geological Society, Bath, U.K.

Ward, P.R.B. (1977), Seiches, tides and wind set-up on Lake Kariba, *Limnol. Oceanogr.,* 24, 151-157.

Wessel, P., and W.H.F. Smith (1996), A global, self-consistent, hierarchical, high-resolution shoreline data base, *J. Geophys. Res.,* 101, 8741-8743.

Figure Captions

1. (left) Map of Loch Ness showing tidal measurement sites (see Table 1a). The two black areas indicate the deepest parts of the loch. (right) Location of Loch Ness in the Highlands of Scotland. IG (Invergordon on the Cromarty Firth, a branch of the Moray Firth) and BF (Beauly Firth, a tidal inlet connected to the head of the Moray Firth) are mentioned in the text.

2. Power spectra of the (a) average and (b) difference of 10-minute pressure time series at the two ends of Loch Ness (sites AL and FA). The ordinates on each plot have the same units with a common arbitrary scaling factor. (Plots made using the MATLAB® *spectrum* function).

3. (a) Vector plot of the observed M_2 tide along the Loch, Circles indicate one standard error. M_2 phase lags are plotted anticlockwise from the abscissa.

(b) Vector plot (mm) of the observed **AL-FA** M_2 tidal-difference (green), together with the difference computed as a combination of loading (blue dashed) and direct (blue solid) components, the blue dashed vector indicating the average of the loading computed from four ocean tide models. The green circle indicates one standard error for the measurements, while the blue circle indicates one standard error due to modelling uncertainties including seasonal changes in M_2 elevations in the North Sea and in water density, uncertainties in nodal M_2 modulation correction and those in loading calculations due to the complicated coastline. On the lower right, the modelling uncertainties blue circle is expanded so as to show more clearly the combined tidal-differences using the individual models: FES2004 (black dot), TPXO7.2 (square), GOT4.7 (triangle) and EOT08a (diamond).

4. The densified grid used for tidal loading calculations following the method of *Bos and Baker* [2005].

5. Cotidal chart for Loch Ness from a numerical tidal model, indicating a small clockwise amphidromic system in the middle of the loch. Co-tidal lines for Greenwich phase lag are shown every 60^0, while co-range lines are drawn every 0.15 mm.

Table 1a. Gauge Types and Locations

Location	Code	Gauge Type	Latitude (°N)	Longitude (°W)
SEPA gauge, below the Caledonian Canal Locks at Fort Augustus	FAS	Float and stilling well	57.145	4.680
Fort Augustus by old railway pier	FA	RBR pressure	57.152	4.670
Tigh na Bruaich by private floating pier	TB	RBR pressure	57.207	4.608
Foyers, south of hydro-electric station	-	RBR pressure (lost)	57.261	4.485
Foyers hydro-electric station (SSE)	FO	Vega acoustic	57.262	4.484
North of Drumnadrochit by lifeboat jetty	DR	RBR pressure	57.337	4.444
Aldourie at Loch outlet, by private pier	AL	RBR pressure	57.407	4.328

Table 1b Principal tidal components observed at each site.

Amplitudes and phases were determined from the complete 201 day measurement period, with standard errors estimated by determining the scatter of each parameter from 7 independent monthly blocks of data divided by √(7-1).

	Amplitude (mm)	Standard Error (mm)	Greenwich phase lag (deg)	Standard Error (deg)
M_2				
FA	**1.98**	0.53	**136.2**	14.5
FAS	**1.33**	0.59	**142.3**	25.6
TB	**1.38**	0.53	**140.0**	20.3
FO	**0.07**	0.62	**168.0**	124.8
DR	**0.48**	0.39	**230.0**	39.4
AL	**1.24**	0.49	**293.5**	23.4
S_2				
FA	**6.34**	1.12	**334.0**	9.9
FAS	**4.16**	0.96	**354.7**	12.8
TB	**6.59**	1.14	**337.7**	11.9
FO	**5.23**	1.12	**328.7**	12.3
DR	**7.01**	1.14	**336.0**	9.1
AL	**7.20**	1.15	**337.6**	9.0
N_2				
FA	**0.51**	0.51	**94.6**	96.1
FAS	**0.37**	0.55	**222.2**	98.0
TB	**0.32**	0.52	**82.4**	176.9
FO	**0.27**	0.59	**58.7**	104.3
DR	**0.07**	0.51	**26.6**	135.4
AL	**0.21**	0.50	**315.5**	74.0

Table 2 Principal tidal components of water level differences between sites.

	Amplitude (mm)	Standard Error (mm)	Greenwich phase lag (deg)	Standard Error (deg)	Distance between sites (km)	Tidal Gradient (mm/km)	Standard Error (mm/km)
M_2							
TB-FA	**0.59**	0.12	**307.7**	10.9	7.00	**0.084**	**0.017**
DR-TB	**1.46**	0.08	**300.7**	3.3	17.50	**0.083**	**0.005**
AL-DR	**1.11**	0.12	**316.4**	6.3	10.25	**0.108**	**0.012**
AL-FA	**3.12**	0.13	**307.5**	2.3	34.75	**0.090**	**0.004**
S_2							
TB-FA	**0.44**	0.10	**24.2**	14.5			
DR-TB	**0.46**	0.13	**311.0**	14.7			
AL-DR	**0.26**	0.08	**16.2**	13.5			
AL-FA	**0.95**	0.10	**354.4**	6.1			
N_2							
TB-FA	**0.28**	0.11	**279.0**	37.5			
DR-TB	**0.28**	0.10	**275.4**	18.2			
AL-DR	**0.23**	0.08	**288.6**	24.4			
AL-FA	**0.80**	0.13	**280.4**	11.4			

Table 3 Amplitudes and phase lags of M_2 tidal loading for each ocean tide model. Phase lags are relative to Greenwich with lags positive.

Tide Model	FES2004		TPXO7.2		GOT4.7		EOT08a	
Site	**Amplitude (mm)**	**Phase lag (deg)**	**Amplitude (mm)**	**Phase lag (deg)**	**Amplitude (mm)**	**Phase lag (deg)**	**Amplitude (mm)**	**Phase lag (deg)**
AL	18.05	147.4	17.85	146.1	18.06	145.0	17.95	146.5
DR	19.12	147.4	18.95	146.2	19.14	145.3	19.02	146.6
FO	19.60	146.6	19.46	145.4	19.64	145.6	19.50	145.8
TB	20.47	146.9	20.34	145.7	20.51	145.1	20.37	146.2
FA and FAS	20.96	146.7	20.84	145.5	21.01	144.9	20.86	146.0
AL-FA	**2.91**	**-37.6**	**2.99**	**-37.7**	**2.96**	**-35.7**	**2.91**	**-36.9**

Figure 1

(left) Map of Loch Ness showing tidal measurement sites (see Table 1a). The two black areas indicate the deepest parts of the loch. (right) Location of Loch Ness in the Highlands of Scotland. IG (Invergordon on the Cromarty Firth, a branch of the Moray Firth) and BF (Beauly Firth, a tidal inlet connected to the head of the Moray Firth) are mentioned in the text.

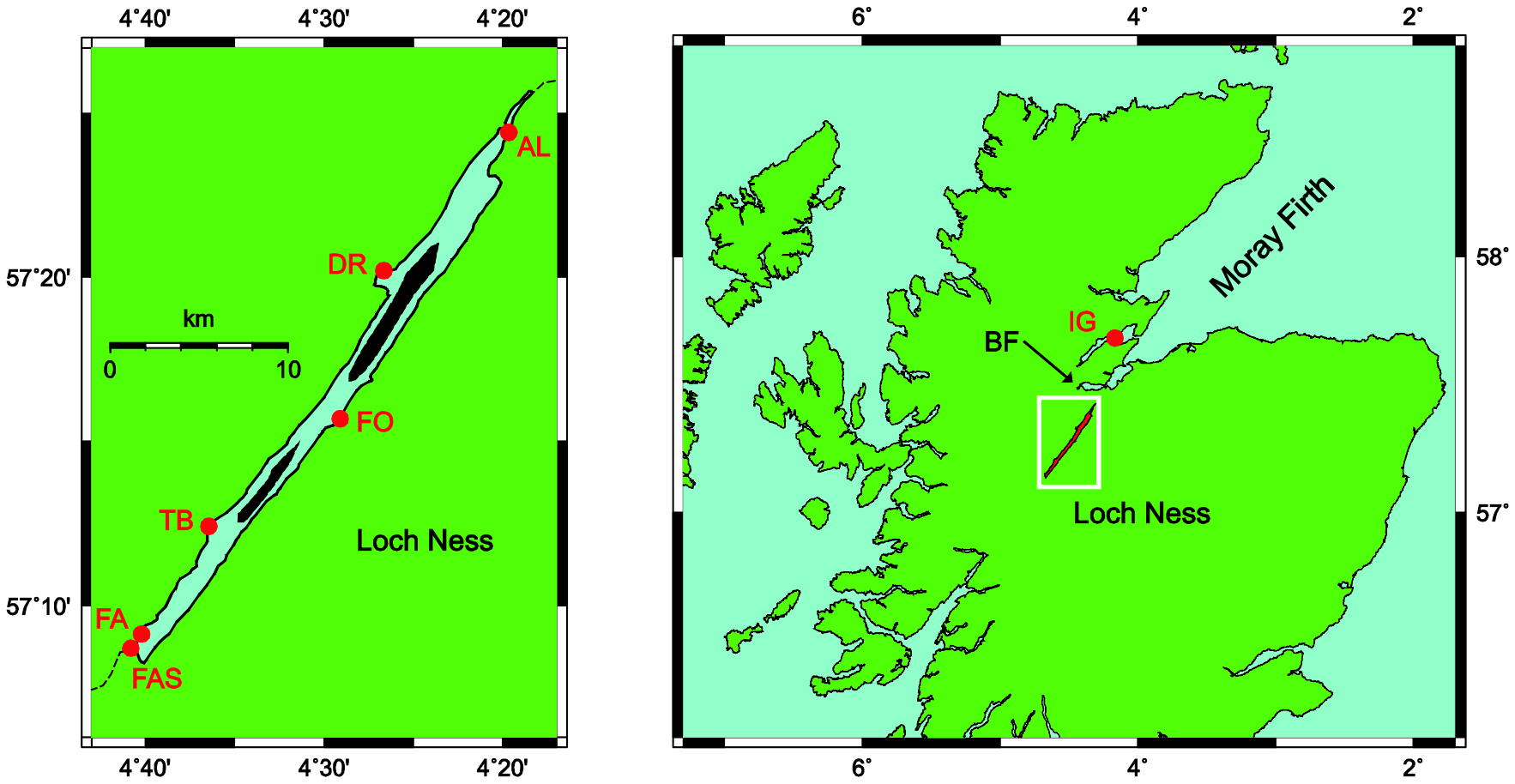
4°40'
4°30'
4°20'
57°20'
57°10'
AL
DR
FO
TB
FA
FAS
km
0
10
Loch Ness
6°
4°
2°
58°
57°
Moray Firth
IG
BF
Loch Ness

Figure 2 on next page

Power spectra of the (a) average and (b) difference of 10-minute pressure time series at the two ends of Loch Ness (sites AL and FA). The ordinates on each plot have the same units with a common arbitrary scaling factor. (Plots made using the MATLAB® *spectrum* function).

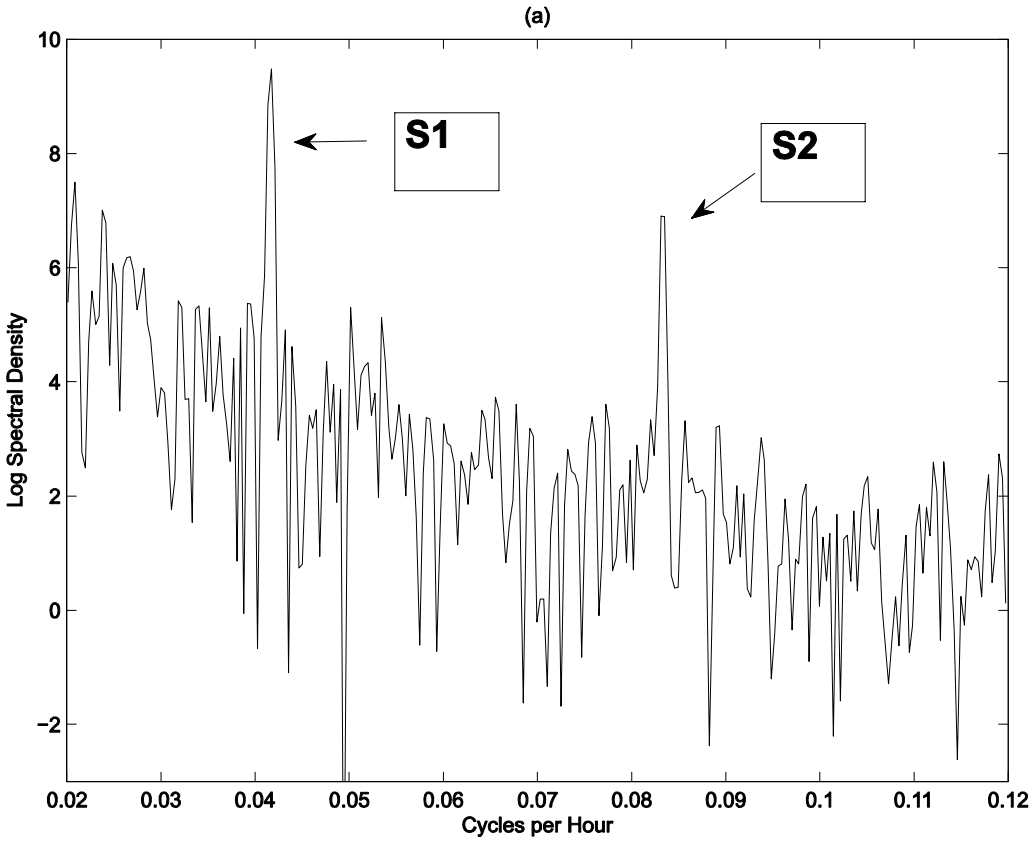
(a)
S1
S2
Log Spectral Density
Cycles per Hour
10
8
6
4
2
0
−2
0.02
0.03
0.04
0.05
0.06
0.07
0.08
0.09
0.1
0.11
0.12

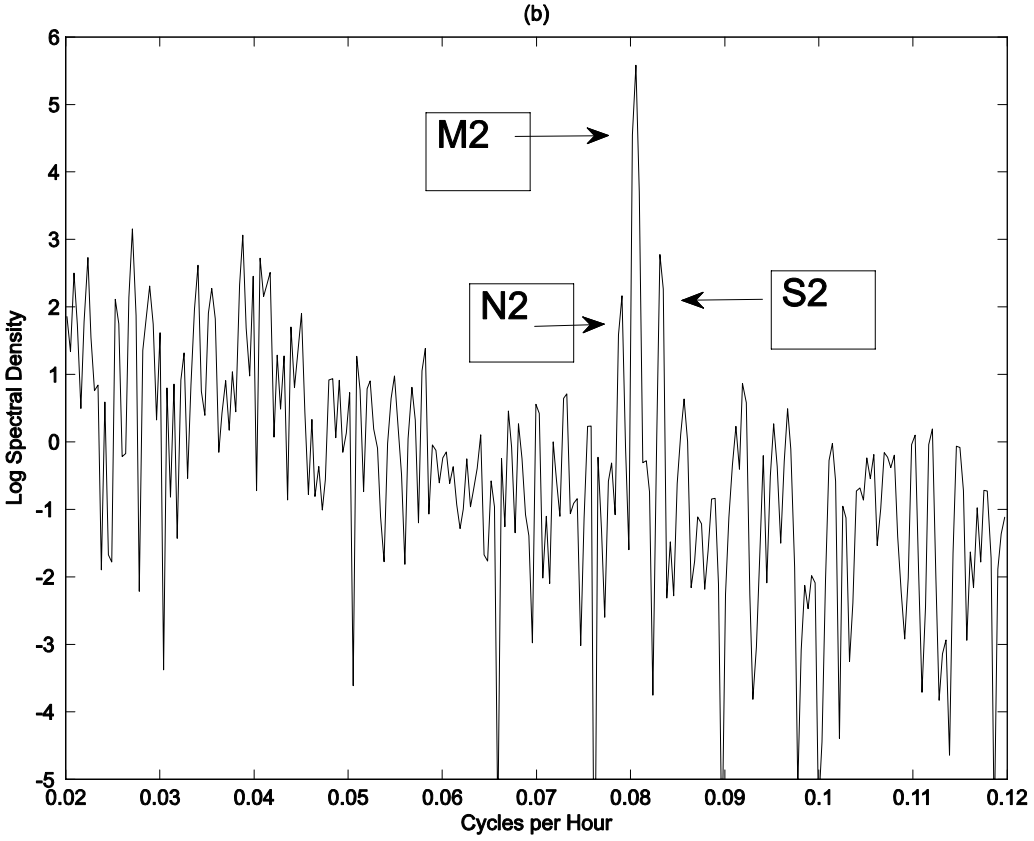
(b)
M2
N2
S2
Log Spectral Density
Cycles per Hour
6
5
4
3
2
1
0
-1
-2
-3
-4
-5
0.02
0.03
0.04
0.05
0.06
0.07
0.08
0.09
0.1
0.11
0.12

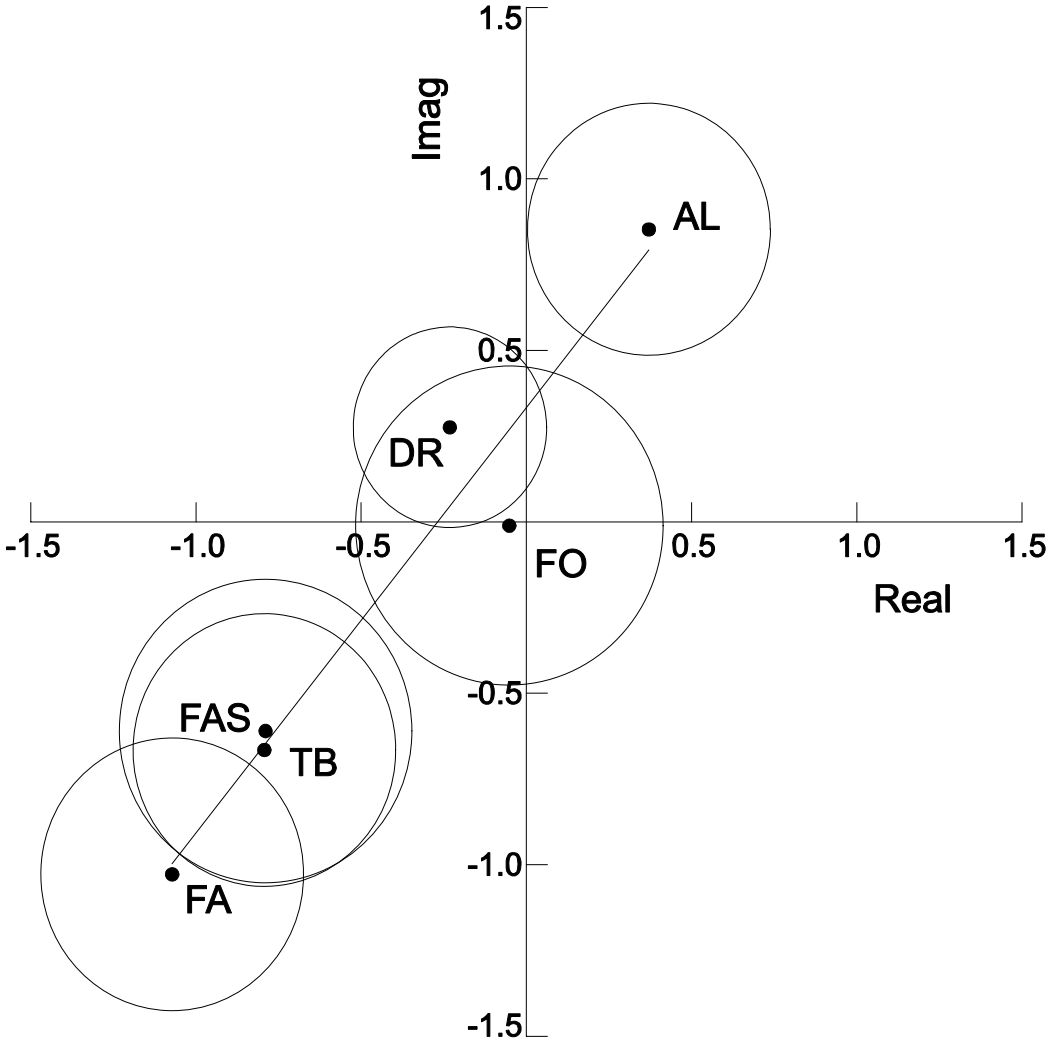

Figure 3a

(a) Vector plot of the observed M_2 tide along the Loch, Circles indicate one standard error. M_2 phase lags are plotted anticlockwise from the abscissa.

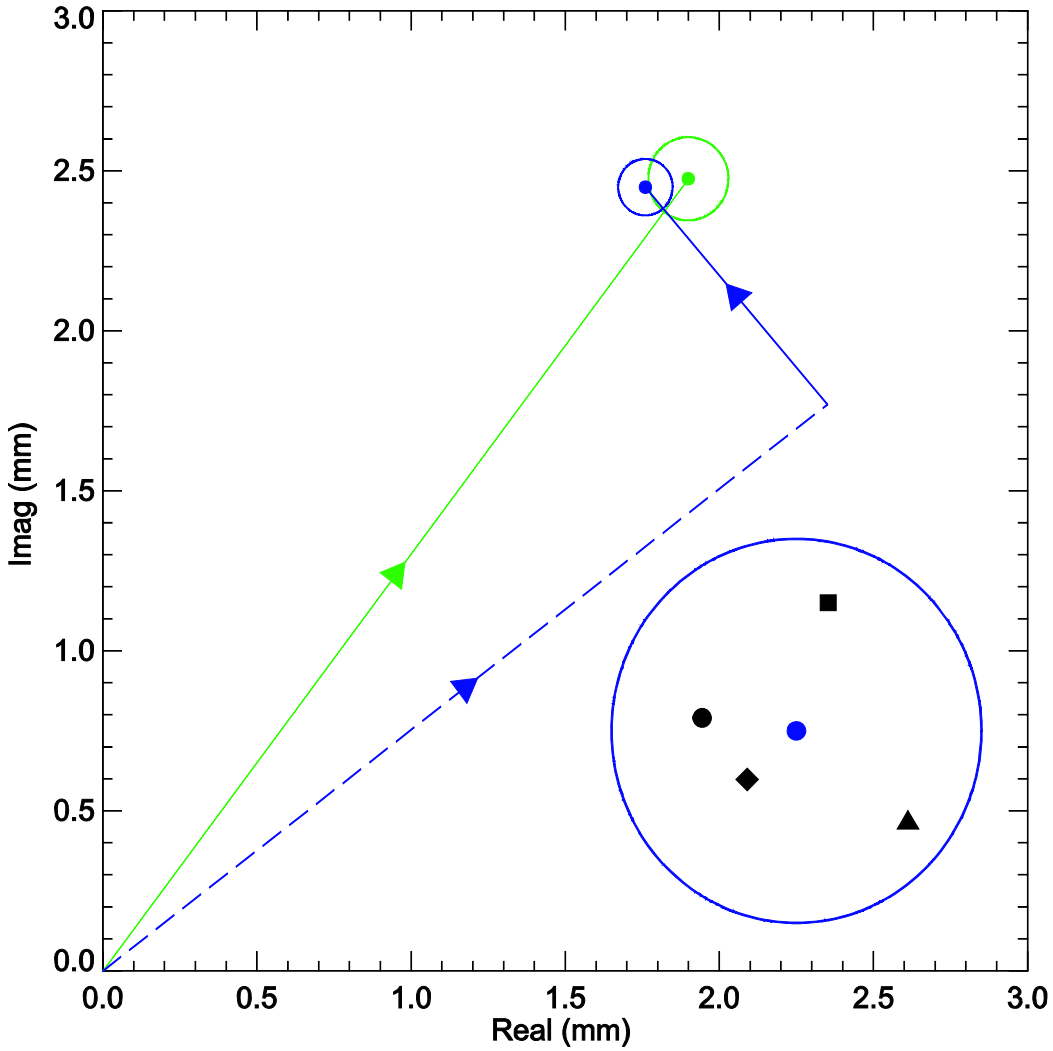

Figure 3b

(b) Vector plot (mm) of the observed **AL-FA** M_2 tidal-difference (green), together with the difference computed as a combination of loading (blue dashed) and direct (blue solid) components, the blue dashed vector indicating the average of the loading computed from four ocean tide models. The green circle indicates one standard error for the measurements, while the blue circle indicates one standard error due to modelling uncertainties including seasonal changes in M_2 elevations in the North Sea and in water density, uncertainties in nodal M_2 modulation correction and those in loading calculations due to the complicated coastline. On the lower right, the modelling uncertainties blue circle is expanded so as to show more clearly the combined tidal-differences using the individual models: FES2004 (black dot), TPXO7.2 (square), GOT4.7 (triangle) and EOT08a (diamond).

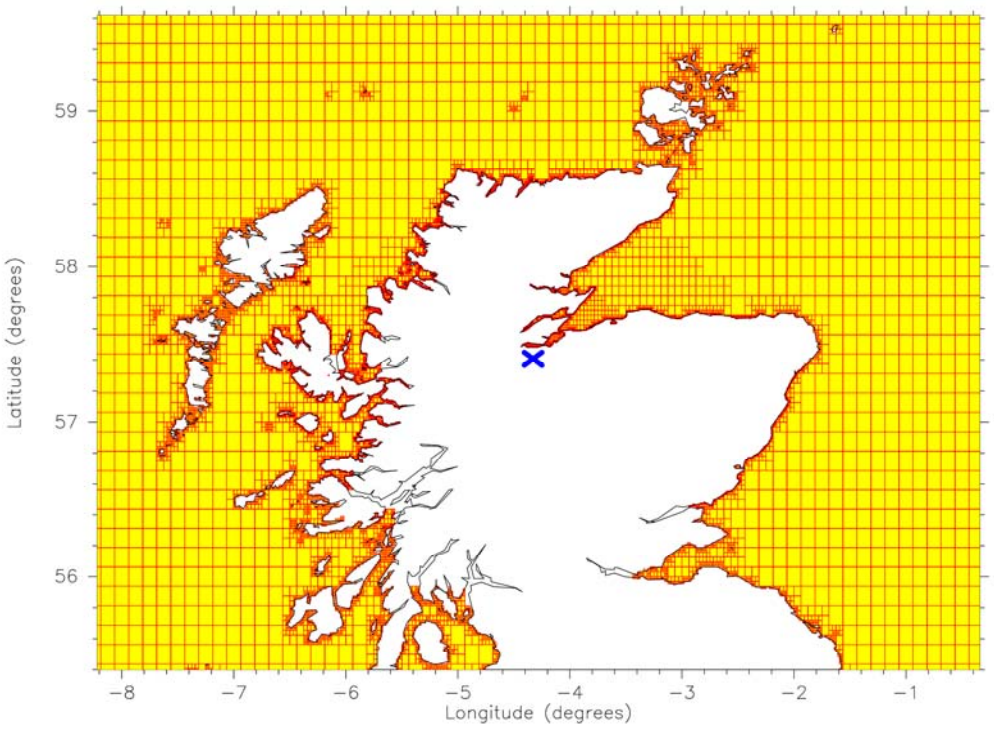

Figure 4

The densified grid used for tidal loading calculations following the method of *Bos and Baker* [2005].

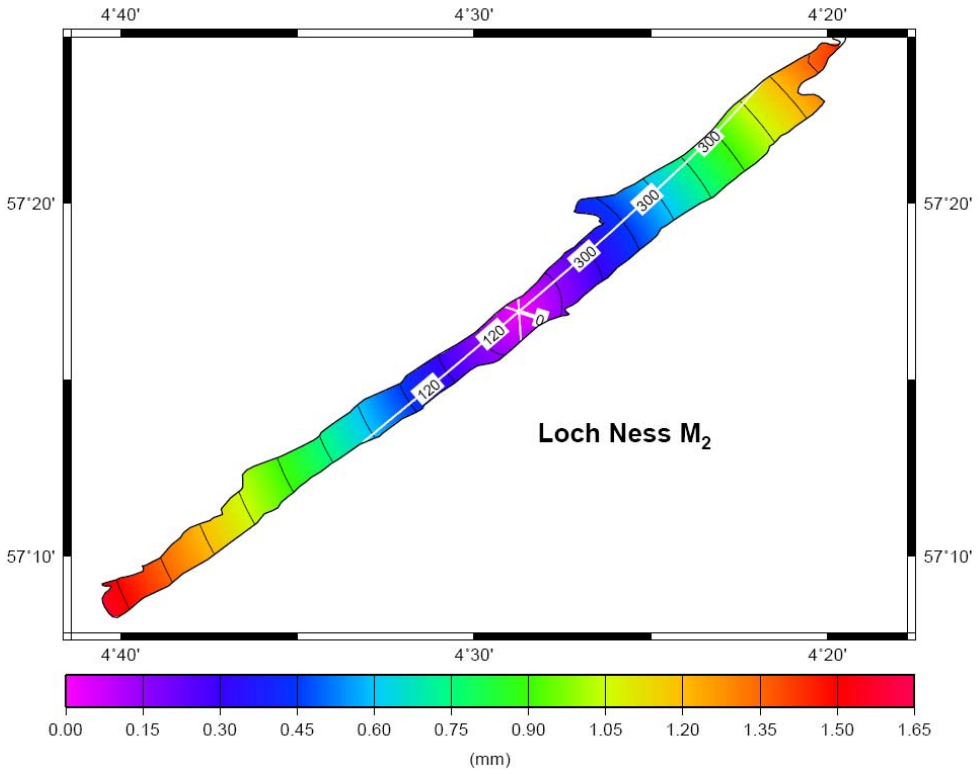

Figure 5

Cotidal chart for Loch Ness from a numerical tidal model, indicating a small clockwise amphidromic system in the middle of the loch. Co-tidal lines for Greenwich phase lag are shown every 60^0, while co-range lines are drawn every 0.15 mm.